

Electron-phonon coupling and exchange-correlation effects in superconducting H_3S under high pressure

Matej Komelj^{1,*} and Henry Krakauer²

¹*Jožef Stefan Institute, Jamova 39, SI-1000 Ljubljana, Slovenia*

²*Department of Physics, College of William and Mary, Williamsburg, VA 23187-8795*

(Dated: November 7, 2018)

We investigate the H_3S phase of sulphur hydride under high pressure $\simeq 200$ GPa by means of *ab-initio* calculations within the framework of the density-functional theory (DFT) with the PBE0 hybrid exchange-correlation (E_{xc}) approximation. The choice of E_{xc} has the largest effect on the calculated electron-phonon coupling (EPC) matrix elements; the high pressure equation of state and phonon frequencies are only slightly modified. Mode-dependent EPC correction factors are determined from PBE0 using a frozen-phonon supercell approach, while standard density-functional perturbation theory is used to determine the EPC with PBE generalized-gradient approximation E_{xc} . Our principle finding is that the calculated PBE0 T_c is enhanced by 25% compared to PBE. This is similar in magnitude, but in opposite direction, to the proposed suppression of T_c by anharmonic effects [Errea *et al.*, *Phys. Rev. Lett.* **114**, 157004 (2015)]. Our calculations demonstrate the importance of considering exchange-correlation approximations for calculations of superconducting properties for this class of materials.

PACS numbers: 74.20.pq, 74.25.Kc, 71.15.Mb

The quest for the holy grail of high-pressure physics, metallic hydrogen, has continued to attract the interest of experimentalists and theorists since Ashcroft proposed that the new phase should exhibit superconductivity with $T_c \sim 270$ K.¹ A recent focus has been on the hydrides where reduced metallization pressures are expected.² Sulphur hydrides have attracted a great deal of attention due to theoretical predictions²⁻⁷ of high $T_c \sim 200$ K under high pressure. This was supported by two experimental reports:^{8,9} superconductivity was first attributed to H_2S in Ref. 8, but Drozdov *et al.*⁹ re-analyzed their measurements, which lead to $T_c \approx 203$ K, now ascribed to the H_3S phase. Theoretically, Li *et al.*³ proposed a metallic phase of hydrogen sulfide H_2S , potentially superconducting with a maximum $T_c \sim 80$ K when subjected to a pressure of 160 GPa. The transition temperature was estimated by applying the Allen-Dynes modified McMillan equation¹⁰ and assuming electron-phonon coupling as the source of superconductivity. Duan *et al.*⁴ performed a systematic investigation of the pressure-dependent $(\text{H}_2\text{S})_2\text{H}_2$ phase diagram and concluded that the cubic $Im\bar{3}m$ H_3S structure was the most stable phase at pressures above 180 GPa, with $T_c \sim 200$ K at 200 GPa. Papaconstantopoulos *et al.*¹¹ applied the Gaspari-Gyorffy theory¹² and argued that superconductivity in H_3S arose mostly from the coupling between the electrons and the H vibrations, whereas the role of the sulphur is to stabilize the hydride at high pressures via hybridization. A similar hypothesis was put forward by Bernstein *et al.*⁵ who proposed that the transport mechanism in the high-pressure H_3S was the same as in MgB_2 . A substantially higher T_c in the hydride could be explained with the considerably smaller atomic masses of the constituents. It has also been argued that the features of the calculated electron-phonon spectrum in H_3S are near optimum for

a high T_c .¹³ Errea *et al.*⁶ claimed, however, that the harmonic approximation, used in the previous calculations, overestimated the electron-phonon coupling and consequently the predicted T_c . Other related candidate materials, such as SeH_3 , have also been investigated.¹⁴ By contrast, Hirsch and Marsiglio¹⁵ have argued against the conventional electron-phonon mechanism and in favor of an electron-hole mediated mechanism.

The previous theoretical investigations³⁻⁷ were based on *ab-initio* calculations that used the semilocal PBE¹⁶ generalized-gradient approximation (GGA). Standard local or semilocal DFT approaches sometimes fail to predict the correct T_c in conventional electron-phonon superconductors because of an insufficient treatment of the exchange-correlation effects.¹⁷⁻¹⁹ In this paper we address the effect of the choice of DFT exchange-correlation functional on the predicted EPC strength. Hybrid DFT (HDFT) methods often improve the predicted properties of materials with hydrogen bonds.^{20,21} In HDFT a fraction of the Hartree-Fock exact-exchange term is added to E_{xc} .²² As a result, HDFT calculations are typically at least an order of magnitude computationally more demanding than local or semilocal E_{xc} . To calculate the effective Kohn-Sham potential for HDFT, it is necessary to evaluate $N_{\mathbf{k}} \times N_{\text{occ}}$ six-dimensional spatial integrals, where $N_{\mathbf{k}}$ and N_{occ} are the number of \mathbf{k} -points and occupied states, respectively. By contrast, only three-dimensional integrals are required for local or semilocal E_{xc} . For this reason, the extension and application of DFT perturbation theory (DFTPT) to calculate electron-phonon coupling coefficients²³ becomes very challenging in HDFT. Instead, we adapted the approximation scheme introduced by Lazzeri *et al.*¹⁷ and Yin *et al.*¹⁹ for GW and HDFT, as described below.

The mode-dependent EPC strengths $\lambda_{\mathbf{q}\nu}$ are given by

$$\lambda_{\mathbf{q}\nu} = \sum_I \frac{1}{M_I \mathcal{N}(\varepsilon_F) \omega_{\mathbf{q}\nu}^2} \sum_{ij} \int \frac{d^3k}{\Omega_{\text{BZ}}} \left| \langle \psi_{\mathbf{k},i} | \frac{dV_{\{\mathbf{R}\}}}{d\mathbf{R}_I} \cdot \mathbf{U}_{\mathbf{q}\nu}^I | \psi_{\mathbf{k}+\mathbf{q},j} \rangle \right|^2 \delta(\varepsilon_{\mathbf{q},i} - \varepsilon_F) \delta(\varepsilon_{\mathbf{k}+\mathbf{q},j} - \varepsilon_F), \quad (1)$$

where the phonon frequencies $\omega_{\mathbf{q}\nu}$ and eigenvectors $\mathbf{U}_{\mathbf{q}\nu}^I$ are obtained by diagonalizing the phonon dynamical matrix; $\varepsilon_{\mathbf{k},i}$, $\psi_{\mathbf{k},i}$ are the single-electron energies and eigenfunctions, $\mathcal{N}(\varepsilon_F)$ is the density of states at the Fermi energy ε_F , and M_I is the mass of the I th atom. The EPC matrix element $\langle \psi_{\mathbf{k},i} | \frac{dV_{\{\mathbf{R}\}}}{d\mathbf{R}_I} \cdot \mathbf{U}_{\mathbf{q}\nu}^I | \psi_{\mathbf{k}+\mathbf{q},j} \rangle$ depends on the change of the self-consistent Kohn-Sham potential with respect to the phonon displacement. All of the quantities in Eq. (1) can be calculated using DFPT^{23–25} for local or semi-local E_{xc} , and this functionality is available in standard codes such a Quantum Espresso.²⁶ Unfortunately, a combination of HFFT and DFPT would be computationally too demanding and has not yet been implemented for solids, to our knowledge. Instead, we use an alternative approach.^{17,19} Supercells and the frozen-phonon method are used to obtain the phonon dynamical matrix and the resulting pairs of $\omega_{\mathbf{q}\nu}$, $\mathbf{U}_{\mathbf{q}\nu}^I$ on a \mathbf{q} -grid commensurate with the supercell.²⁷ Small but finite phonon displacements can then be introduced to obtain phonon-induced Kohn Sham potentials, which can be expressed to first order as: $V_{\{\mathbf{R}\}} + (dV_{\{\mathbf{R}\}}/d\mathbf{R}_I) \cdot \mathbf{U}_{\mathbf{q}\nu}^I$. The change $\Delta\varepsilon$ of a single-electron energy is approximated as:

$$\Delta\varepsilon \approx \left\langle \frac{dV_{\{\mathbf{R}\}}}{d\mathbf{R}_I} \cdot \mathbf{U}_{\mathbf{q}\nu}^I \right\rangle. \quad (2)$$

The difference $\Delta\varepsilon$ describes band splitting due to the lifted degeneracy in the presence of the phonon. For the application of the approximation (2) for the calculation of $\lambda_{\mathbf{q}\nu}$ only the splittings nearest to the Fermi level are relevant. An example is presented in Fig. 1 for $Im\bar{3}m$ H₃S in the presence of phonon mode $\nu = 6$ at $\mathbf{q} = 0$, calculated with PBE E_{xc} .

The band splittings are determined for both DFT and HFFT, $\Delta\varepsilon_{\mathbf{q}\nu}^{\text{DFT}}$ and $\Delta\varepsilon_{\mathbf{q}\nu}^{\text{HFFT}}$, respectively. Using Eq. (2) in Eq. (1) for DFT and for HFFT yields the following approximation to estimate the HFFT electron-phonon coupling coefficients:

$$\lambda_{\mathbf{q}\nu}^{\text{HFFT}} \approx \lambda_{\mathbf{q}\nu}^{\text{DFT}} f_{\mathbf{q}\nu}, \quad (3)$$

where the correction factor $f_{\mathbf{q}\nu}$ is given by:

$$f_{\mathbf{q}\nu} = \frac{\mathcal{N}^{\text{DFT}}(\varepsilon_F^{\text{DFT}})}{\mathcal{N}^{\text{HFFT}}(\varepsilon_F^{\text{HFFT}})} \left(\frac{\omega_{\mathbf{q}\nu}^{\text{DFT}}}{\omega_{\mathbf{q}\nu}^{\text{HFFT}}} \right)^2 \left(\frac{\Delta\varepsilon_{\mathbf{q}\nu}^{\text{HFFT}}}{\Delta\varepsilon_{\mathbf{q}\nu}^{\text{DFT}}} \right)^2. \quad (4)$$

This procedure could be repeated, in principle, to determine $\lambda_{\mathbf{q}\nu}^{\text{HFFT}}$ for each phonon mode throughout the Brillouin zone (BZ), using appropriate \mathbf{q} -commensurate supercells. We note, however, that the Allen-Dynes equation for the superconducting transition temperature¹⁰

$$T_C = \frac{\omega_{\text{log}}}{1.2} \exp \left(\frac{-1.04(1 + \lambda)}{\lambda - \mu^*(1 + 0.62\lambda)} \right) \quad (5)$$

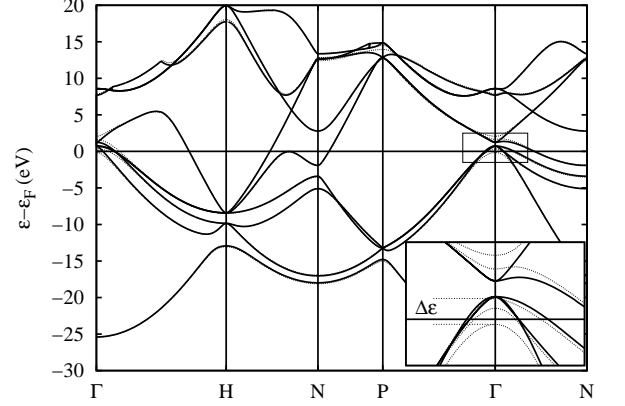


FIG. 1. Band splitting due the presence of a phonon. PBE band structures of $Im\bar{3}m$ H₃S are shown: solid lines correspond to the undistorted crystal, and dashed lines are for the atoms displaced according to the phonon mode $\nu = 6$ at $\mathbf{q} = 0$. The inset presents the details of the band splitting close to the Fermi energy near the Γ point due to the lifted degeneracy caused by the presence of the phonon.

depends on the total electron-phonon coupling coefficient λ , which is given by an integral over the BZ and sum over phonon branches: $\lambda = (1/\Omega_{\text{BZ}}) \sum_{\nu} \int \lambda_{\mathbf{q}\nu} d^3q$, where Ω_{BZ} is the volume of the BZ; μ^* and ω_{log} are discussed below. Therefore we determine the center of gravity \mathbf{q}_{ν}^* in the irreducible wedge of the Brillouin zone (IBZ) with respect to the $\lambda_{\mathbf{q}\nu}^{\text{DFT}}$ for each DFT phonon branch ν :

$$\mathbf{q}_{\nu}^* = \frac{\int_{\text{IBZ}} d^3q \lambda_{\mathbf{q}\nu}^{\text{DFT}} \mathbf{q}}{\int_{\text{IBZ}} d^3q \lambda_{\mathbf{q}\nu}^{\text{DFT}}}. \quad (6)$$

For each branch we calculate the correction factor (4) $f_{\mathbf{q}^*\nu}$ and use this single value for all \mathbf{q} -points within a given branch ν :

$$\lambda_{\mathbf{q}\nu}^{\text{HFFT}} \approx \lambda_{\mathbf{q}\nu}^{\text{DFT}} f_{\mathbf{q}^*\nu} \quad (7)$$

The calculations were carried out by applying the Quantum Espresso²⁶ code. The DFT exchange-correlation potential was PBE, whereas for HFFT we used PBE0.^{28,29} The bare electron-ion interactions were described with the norm-conserving Goedecker-Hartwigsen-Hutter-Teter^{30,31} pseudopotentials. The planewave and charge-density cut-off parameters were set to 476 eV and 1904 eV, respectively. A Monkhorst-Pack³² $16 \times 16 \times 16$ \mathbf{k} -point grid was used for the BZ integration primitive cell calculations. PBE0 phonon

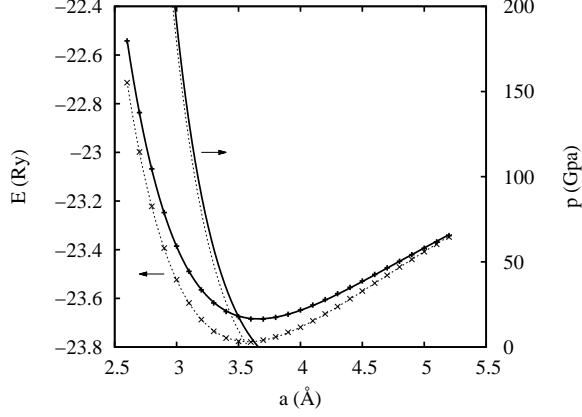


FIG. 2. The calculated total energy with respect to the lattice parameter a for PBE (+) and PBE0 (x) fitted with the Birch-Murnaghan equation of state, from which the pressure was calculated. The solid lines are for PBE, the dashed lines are for PBE0.

spectra were calculated using the frozen-phonon method as implemented in the Phonopy²⁷ code, whereas the DFT electron-phonon coefficients were determined using DFPT, which is a part of the Quantum Espresso package. The total electron-phonon coupling coefficient λ^{DFT} was obtained by using a $4 \times 4 \times 4$ \mathbf{q} -point grid in the BZ. The force constants for the frozen-phonon method were obtained from a $2 \times 2 \times 2$ -supercell calculation.

Fig. 2 presents the calculated total energies as a function of the lattice parameter a fitted with the Birch-Murnaghan equation of state.³³ The difference between PBE and PBE0 is most pronounced at zero pressure, reflecting the $\simeq 2\%$ difference in equilibrium lattice parameters: 3.66 Å and 3.58 Å, respectively. Near 200 GPa, however, PBE and PBE0 yield very similar lattice parameters, which match the published⁴ value 2.984 Å. We used this value for the subsequent calculations of the phonon-related properties.

The effect of HDFT is larger for phonon frequencies near 200 GPa, as shown in Fig. 3. The largest differences are for the optic modes, especially near the N point, while differences for the acoustic modes are small. PBE EPC strengths throughout the Brillouin zone are depicted in Fig. 4. In contrast to the case of BaBiO₃ from Ref. 19, there are no distinguished points with particularly large values of $\lambda_{\mathbf{q}\nu}^{\text{DFT}}$. This provides some justification for our introduction here of the center of gravity point \mathbf{q}^* in Eq. (5). Using this approximation, the number of HDFT $f_{\mathbf{q}\nu}$ evaluations is reduced from 96 (the number of \mathbf{q} -points in the irreducible BZ times the number of bands) to only 12 (the number of bands) in Eqs. (4) and (6). For all phonon branches, the center of gravity point is well-approximated by either $\mathbf{q}^* = \Gamma$ or $\mathbf{q}^* = (0, 0, 1/2) 2\pi/a$. The band splittings $\Delta\epsilon$ can therefore be obtained from

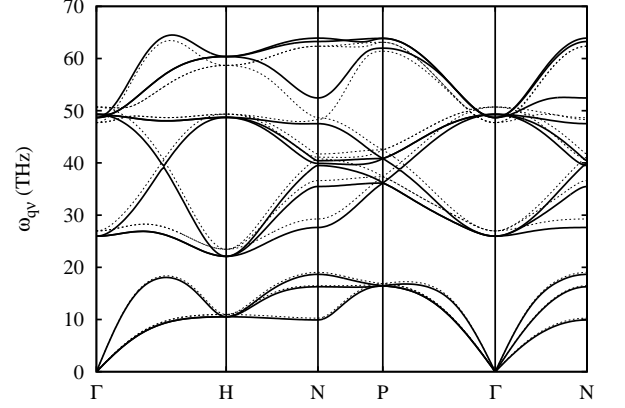


FIG. 3. Calculated phonon dispersion for the PBE (solid lines) and PBE0 (dashed lines) exchange-correlation potentials.

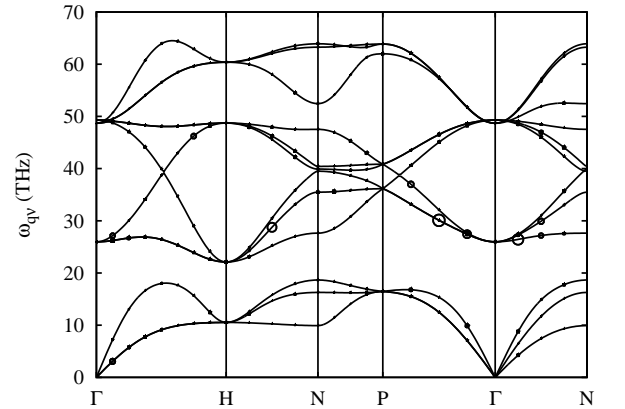


FIG. 4. Electron-phonon \mathbf{q} -dependent PBE coupling strengths: the size of the circles, superimposed on the phonon dispersion curves, is proportional to the electron-phonon coupling coefficient $\lambda_{\mathbf{q}\nu}^{\text{DFT}}$.

primitive cell or $1 \times 1 \times 2$ -supercell calculations, respectively.

A suitable indicator for the overall influence of the exchange-correlation effects on the electron-phonon coupling is the Eliashberg spectral function $\alpha^2 F(\omega) \propto \sum_{\nu} \int (1/\Omega_{\text{BZ}}) \lambda_{\mathbf{q}\nu} \omega_{\mathbf{q}\nu} \delta(\omega - \omega_{\mathbf{q}\nu}) d^3q$ which is plotted in Fig. 5 (using gaussians with width $\sigma = 0.5$ THz to represent the δ -functions). The difference in peak positions reflects the changes in phonon dispersion in Fig. 3. The highest peaks are located in the middle of the frequency range, which is in agreement with the distribution of the $\lambda_{\mathbf{q}\nu}^{\text{PBE}}$ magnitudes in Fig. 4. The PBE0 peaks for

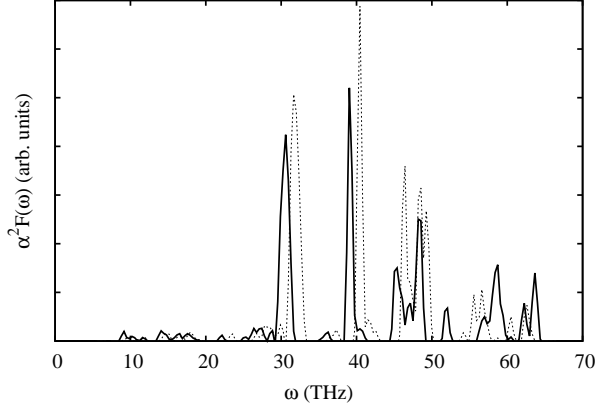


FIG. 5. The calculated Eliashberg spectral function $\alpha^2 F(\omega)$, using PBE (solid lines) and the PBE0 (dashed lines) exchange-correlation potentials.

	λ	$\omega_{\log} [K]$	$T_c [K]$
PBE	1.76	1657	217-201
PBE0	2.18	1773	270-253

TABLE I. A comparison between the PBE and PBE0 calculated quantities, which appear in the Allen-Dynes equation (5), and between the resulting T_c for the retarded Coulomb repulsion $\mu^* = 0.1 - 0.13$.

frequencies up to 50 THz are higher than the corresponding PBE peaks, which is due to the enhanced phonon-induced band splitting in PBE0 [Eq. (4)]. The situation is the opposite at the frequencies higher than 50 THz, where the PBE peaks are higher.

The quantitative results are summarized in Table I. The superconducting transition temperature T_c in the Allen-Dynes equation (5) depends not only on the electron-phonon coupling coefficient λ , but also on the logarithmic average frequency $\omega_{\log} = (1/\lambda\Omega_{\text{BZ}}) \sum_{\nu} \int \lambda_{\mathbf{q}\nu} \log(\omega_{\mathbf{q}\nu}) d^3q$ and the retarded Coulomb repulsion μ^* . Here, we simply adopt literature values for μ^* .¹¹ From visual inspection of Fig. 3 it is not evident whether PBE0 yields higher or lower phonon frequencies on average than PBE. Indeed, the calculated ω_{\log} values differ by only 7%. Thus, the change in phonon frequencies has only a small effect on the PBE0 enhancement of λ by 24%. A comparable enhancement of λ was also found for graphene/graphite¹⁷ and C₆₀ molecule.¹⁸ As shown in the Table, the calculated PBE0 T_c , using the Allen-Dynes equation, is higher by about 25% compared to PBE. The influence of the exchange-correlation effects on the μ^* is complex, and it is not in the focus of the present paper. DFT and

Hartree-Fock (and thus also HDFT) wave functions differ only slightly,³⁴ so the double Fermi-surface averaged electron-electron Coulomb interactions will be similar. Since these determine μ and μ^* ,³⁵ it is reasonable to compare predictions of DFT and HDFT using the same μ^* . On the basis of the presented results it is clear that the predicted T_c would be enhanced for any reasonable change in μ^* after switching from PBE to PBE0.

The context for our results is the theory of conventional electron-phonon superconductivity as described by DFT. In H₃S and related sulfides, the normal-state Fermi liquid quasiparticles have been described by DFT band structures and wave functions, using PBE E_{xc} . The DFT approximation is often quite good and is widely used, although there are no guarantees regarding the accuracy of the related one-particle Kohn-Sham eigenstates. Phonon excitations are commonly described in the harmonic approximation, using DFPT or DFT supercell calculations. These are ground state properties, within the Born-Oppenheimer approximation, so DFT is well justified. Using DFT for the non-adiabatic EPC is also justified within Migdal's theorem,^{35,36} and these are treated, as described above. The superconducting transition temperature T_c is then usually estimated using the McMillan or Allen-Dynes equations, although the superconducting anisotropic gap equation can be used^{7,14,23,37} by means of SCDFT. The SCDFT calculation with harmonic phonons¹⁴ yielded $T_c = 180$ K for H₃S, in agreement with experiment. While SCDFT provides a sound footing for the DFT treatment of superconductivity, it does not in itself improve the electronic band structure and phonon properties. The effects of anharmonicity were studied by Errea *et al.*⁶ They found that anharmonicity suppressed λ by 30%; T_c was suppressed by 34 and 56 K, respectively, using the McMillan equation or the isotropic Migdal-Eliashberg equations. All of these studies were based on PBE E_{xc} . Here we have shown that the choice of exchange-correlation potential can have effects of similar magnitude on the EPC and T_c . The present PBE0 calculations modify the electronic quasiparticles in the theory, the phonon excitations, and the EPC. For T_c , we relied on the Allen-Dynes equations with our calculated PBE0 λ and phonon frequencies.

In summary, we examined the influence of exchange-correlation effects on the electron-phonon coupling in cubic $Im\bar{3}m$ H₃S under high pressure. We introduced the electron-phonon coupling center-of-gravity point \mathbf{q}^* , modifying the approach used in Ref. 19. We calculated a 25% enhancement of T_c for HDFT compared to PBE predictions. This is similar in magnitude, but in opposite direction, to the proposed suppression of T_c by anharmonic effects in Ref. 6. Our results demonstrate the importance of considering exchange-correlation approximations for calculations of superconducting properties for this class of materials.

ACKNOWLEDGMENTS

We thank Dimitrios A. Papaconstantopoulos for helpful discussions and Eric J. Walter for consultations on the

computer calculations. HK acknowledges support from ONR (N000141211042). We also acknowledge computing support from the computational facilities at William and Mary.

-
- * matej.komelj@ijs.si
Visiting scientist at the College of William and Mary
- ¹ N. W. Ashcroft, Phys. Rev. Lett. **21**, 1748 (1968).
 - ² N. W. Ashcroft, Phys. Rev. Lett. **92**, 187002 (2004).
 - ³ Y. Li, J. Hao, H. Liu, Y. Li, and Y. Ma, The Journal of Chemical Physics **140**, 174712 (2014).
 - ⁴ D. Duan, Y. Liu, F. Tian, D. Li, X. Huang, Z. Zhao, H. Yu, B. Liu, W. Tian, and T. Cui, Sci. Rep. **4**, 6968 (2014).
 - ⁵ N. Bernstein, C. S. Hellberg, M. D. Johannes, I. I. Mazin, and M. J. Mehl, Phys. Rev. B **91**, 060511 (2015).
 - ⁶ I. Errea, M. Calandra, C. J. Pickard, J. Nelson, R. J. Needs, Y. Li, H. Liu, Y. Zhang, Y. Ma, and F. Mauri, Phys. Rev. Lett. **114**, 157004 (2015).
 - ⁷ R. Akashi, M. Kawamura, S. Tsuneyuki, Y. Nomura, and R. Arita, Phys. Rev. B **91**, 224513 (2015).
 - ⁸ A. P. Drozdov, M. I. Erements, and I. A. Trojan, (), arXiv:1412.0460.
 - ⁹ A. P. Drozdov, M. I. Erements, I. A. Trojan, V. Ksenofontov, and S. I. Shylin, Nature **525**, 73 ().
 - ¹⁰ P. B. Allen and R. C. Dynes, Phys. Rev. B **12**, 905 (1975).
 - ¹¹ D. A. Papaconstantopoulos, B. M. Klein, M. J. Mehl, and W. E. Pickett, Phys. Rev. B **91**, 184511 (2015).
 - ¹² G. D. Gaspari and B. L. Gyorffy, Phys. Rev. Lett. **28**, 801 (1972).
 - ¹³ E. J. Nicol and J. P. Carbotte, Phys. Rev. B **91**, 220507 (2015).
 - ¹⁴ J. A. Flores-Divas, A. Sanna, and E. K. U. Gross, ArXiv:1501.06336v1.
 - ¹⁵ J. Hirsch and F. Marsiglio, Physica C: Superconductivity and its Applications **511**, 45 (2015).
 - ¹⁶ J. P. Perdew, K. Burke, and M. Ernzerhof, Phys. Rev. Lett. **77**, 3865 (1996).
 - ¹⁷ M. Lazzeri, C. Attaccalite, L. Wirtz, and F. Mauri, Phys. Rev. B **78**, 081406 (2008).
 - ¹⁸ J. Laflamme Janssen, M. Côté, S. G. Louie, and M. L. Cohen, Phys. Rev. B **81**, 073106 (2010).
 - ¹⁹ Z. P. Yin, A. Kutepov, and G. Kotliar, Phys. Rev. X **3**, 021011 (2013).
 - ²⁰ Y. Okamoto, M. Saito, and A. Oshiyama, Phys. Rev. B **58**, 7701 (1998).
 - ²¹ H. Shi, N. Zarifi, W.-L. Yim, and J. S. Tse, Journal of Physics: Conference Series **377**, 012093 (2012).
 - ²² A. D. Becke, J. Chem. Phys. **98**, 1372 (1993).
 - ²³ M. Lüders, M. A. L. Marques, N. N. Lathiotakis, A. Floris, G. Profeta, L. Fast, A. Continenza, S. Massidda, and E. K. U. Gross, Phys. Rev. B **72**, 024545 (2005).
 - ²⁴ S. Baroni, P. Giannozzi, and A. Testa, Phys. Rev. Lett. **58**, 1861 (1987).
 - ²⁵ X. Gonze and C. Lee, Phys. Rev. B **55**, 10355 (1997).
 - ²⁶ P. Giannozzi, S. Baroni, N. Bonini, M. Calandra, R. Car, C. Cavazzoni, D. Ceresoli, G. L. Chiarottia, M. Cococcioni, I. Dabo, A. D. Corso, S. Fabris, G. Fratesi, S. de Gironcoli, R. Gebauer, U. Gerstmann, C. Gougoussis, A. Kokalj, M. Lazzeri, L. Martin-Samos, N. Marzari, F. Mauri, R. Mazzarello, S. Paolini, A. Pasquarello, L. Paulatto, C. Sbraccia, S. Scandolo, G. Sclauzero, A. P. Seitsonena, A. Smogunov, P. Umari, and R. M. Wentzcovitch, J. Phys. Condens. Matter **21**, 395502 (2009).
 - ²⁷ A. Togo, F. Oba, and I. Tanaka, Phys. rev. B **78**, 134106 (2008).
 - ²⁸ J. P. Perdew, M. Ernzerhof, and K. Burke, The Journal of Chemical Physics **105**, 9982 (1996).
 - ²⁹ C. Adamo and V. Barone, The Journal of Chemical Physics **110**, 6158 (1999).
 - ³⁰ C. Hartwigsen, S. Goedecker, and J. Hutter, Phys. Rev. B **58**, 3641 (1998).
 - ³¹ S. Goedecker, M. Teter, and J. Hutter, Phys. Rev. B **54**, 1703 (1996).
 - ³² H. J. Monkhorst and J. Pack, Phys. Rev. B **13**, 5188 (1976).
 - ³³ F. Birch, Phys. Rev. **71**, 809 (1947).
 - ³⁴ R. Stowasser and R. Hoffmann, Journal of the American Chemical Society **121**, 3414 (1999).
 - ³⁵ P. B. Allen and B. Mitrovich, in *Solid State Physics, Vol 37*, edited by F. Seitz, D. Turnbull, and H. Ehrenreich (Academic Press, New York, 1982) pp. 1–92.
 - ³⁶ A. B. Migdal, Sov. Phys. JETP, **996** (1958).
 - ³⁷ A. Sanna, G. Profeta, A. Floris, A. Marini, E. Gross, and S. Massidda, Physical Review B **75**, 020511 (2007).